Journal of Computational Applied Mechanics 2022, 53(4): 626-638

DOI: 10.22059/jcamech.2022.347816.748

RESEARCH PAPER

Multilayer Hydrogel Seals: Numerical Study of Elastic Leak

Ali Akbar Abbasian Arani, Houshang Barkhordari*

Mechanical Engineering Faculty, University of Kashan, Kashan, Iran

Abstract

Utilizing hydrogels for sealing devices has attracted the attention of researchers in both academia and industry. The main reason for this attraction is the ability of these materials to absorb surrounding fluid and swelling and the subsequent sealing of the desired portion without any external manipulation. Investigation of the behavior of these materials when implemented as seals is of major importance. This paper studies a rectangular multilayer hydrogel with different material properties numerically by using thermo-mechanical coupled constitutive models available in the literature. Leakage models of elastomeric seals were implemented to examine the leakage of these seals under the pressure of the fluid. The methods are validated through comparison with experiments benchmarked in the literature. After modeling the seals, the mechanism of leakage is investigated, and parameter study of seals considering the cross-linking density distribution of multilayer hydrogel is presented. The findings showed that the ascending and descending property distributions in the studied multilayer hydrogel have a considerable effect on sealing behavior, providing the researchers with an accurate vision of designing such seals.

Keywords: Hydrogel, Leakage, Multilayer, Numerical Method.

1. Introduction

Hydrogels, as smart polymeric materials with a 3D long-chain cross-linking network can imbibe in water, absorb a vast amount of water, and swell. Response to wireless stimuli such as temperature[1, 2] pH [3-5] light intensity [6-8] and magnetic field [9] changes is another remarkable characteristic of these materials. The diffusion of aquatic solvent molecules into the polymeric chain increases hydrogel swelling. The mentioned abilities of hydrogel have attracted researchers' attention to applying this material in microfluidics [10, 11], soft robotics [12, 13], channel sealing [11, 14], and smart actuators devices [15-61]. In addition, the biocompatibility of hydrogels allows them to be used in drug delivery [62], mechanobiology [63], and tissue engineering[64-66]. Sealing is an important application of elastomers where the gap between a channel or a pipe made of stiff material can be filled, preventing fluid passage through the gap. Hydrogels as a smart elastomeric material have recently been used as seals that in some cases, do not react to physical or chemical stimuli. Due to their ability to absorb surrounding solvents and swelling, they can automatically produce the necessary contact stress [67, 68]. Beebe et al.[3] were the pioneer in presenting hydrogel micro-valve in response to the pH-stimuli in order to control fluid flow in microfluidic systems. Accordingly, the industrial application of swellable elastomeric micro-valves[3, 67, 69, 70] has been studied alongside academic investigations.

A constitutive model of hydrogels is essential to define and analyse their complex and nonlinear behavior. Modeling hydrogel behavior with different sensitivities to external stimuli [71-74] has been introduced. Hong et al [75]

* Corresponding author. Tel.: 09167208505; fax: 09160931361.
E-mail address: h.barkhordari2022@gmail.com

proposed a coupled thermo-mechanical model for predicting hydrogel sealing behavior in contact with fluid flow and considering large deformation. In their model, the free energy from mixing the solvent with polymer chains and mechanical deformation of the polymer network conform to the Flory-Rehner theory [76]. They assumed the Neo-Hookean model along with the Flory-Huggins model for the two mentioned free energy densities [77, 78]. Moreover, the kinetics of the generated contact stress and swelling behavior of these polymeric sealing materials were employed [79, 80]. In the following references [11, 67, 81], the principle of leakage mechanism in such seals is studied comprehensively. Lou et al. [82] investigated the effect of the geometrical parameters on its contact stress considering hydrogel swelling.

Recently, the application of layered smart actuators has attracted the attention of researchers. Smart polymeric-sensitive materials can be attached to the natural or two elastomer layers to create a bilayer for single-way and double-way bending sensors [83, 84]. Another way for layering is using functionally graded (FG) material by distributing different material properties in the thickness direction for micro-beams or in the radius direction for micro-valves made of pH/temperature-sensitive hydrogel [85-89].

Due to the importance of the multilayer approach in hydrogel performance, the current study comprehensively investigated the behavior of a multilayer hydrogel resting from the bottom of the channel in a way that may affect sealing (Figure 1). Unlike the outdated micro-channels that used a moving part as an upper side of the channel to compress elastomer for sealing, this study uses a rectangular hydrogel in contact with water molecules to absorb them and swell, producing sufficient contact stress for complete sealing (Figure 1). This approach lowers the cost of manufacturing and facilitates the procedure. It should be noted that the seal failure might generate leakage even if seals are not expensive in these structures [11], necessitating attention to designing and behavior recognition of elastomer sealing. The effect of layering hydrogel with different material distribution in two approaches of descending and ascending for channel sealing has been analyzed by considering parameter variations.

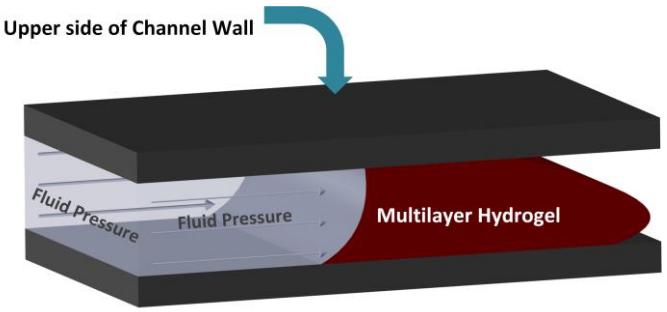

Figure 1: Schematic of multilayer hydrogel seal in contact with fluid pressure

The paper is organized as follows. In Section 1, a comprehensive literature review is presented. Then, the model description containing thermo-mechanical behavior and the results of the model are confirmed with experiments benchmarked in the literature. The validity of the proposed model is discussed in Section 2. The leakage mechanism is introduced in detail in Section 3. The comparison involves the hydrogel contact stress under the irradiation of different channel pressures. After validation, some applicable parameters of the sealing behavior of hydrogel (e.g., an RTG) and the effect of the multilayer hydrogel length are investigated numerically in Section 4. Also, the initial and deformed configurations of the proposed elastomeric seal are illustrated in different steps under fluid pressure. Finally, conclusions are drawn in Section 5.

2. Multilayer Hydrogel Modelling

The swelling behavior of multilayer hydrogel in a rectangular shape is presented by W_s, and W_m represents the additive decomposition of free energy density for elastic and mixing parts. The mentioned elastic and mixing parts follow the Neo-Hookean and Flory-Huggins models. Hydrogel as a hyperelastic material is expressed as follows [75]:

$$W(\mathbf{F},C) = \underset{\text{Decompostion of Free energy}}{\downarrow} \quad \underset{\text{Mixing part}}{W_m(C)} \quad + \quad \underset{\text{Elastic(Stretch) Part}}{W_s(\mathbf{F})} \qquad (1)$$

Based on the Neo-Hookean model, the deformation of multilayer hydrogel is employed this way:

$$W_s(F) = \frac{1}{2} N k_B T (I_1 - 3 - 2\log(J)) \qquad (2)$$

where T, N, and K_B are the absolute temperature, the polymer chain density, and the Boltzmann constant ($K_B = 1.38\times10^{-3} JK^{-1}$), and the specific term of NkT in the dry state represents the shear modulus calculated through $NKT = 1kpa - 10Mpa$ [75]. Considering the Lagrangian perspective, the gradient deformation tensor ($\boldsymbol{F}$) is introduced by two states: dry (reference) and deformed states. When the network is in a dry state, it is considered as the initial position (x) and the current state X(x). The right Cauchy-Green deformation gradient is defined as:

$$\mathbf{C} = \mathbf{F}^T \mathbf{F} \qquad (3)$$

In continuation, I_1 and J are the first invariant of the right Cauchy–Green deformation tensor and the determinant of the deformation gradient $\boldsymbol{F}$.

As mentioned, Flory-Huggins models as the extended formulation for defining the mixing part of the decomposition of free energy density into the hydrogel network W_m is employed as below:

$$W_m(C) = -\frac{k_B T}{\nu}\left[\nu C \ln\left(1+\frac{1}{\nu C}\right)+\frac{\chi}{1+\nu C}\right] \qquad (4)$$

In equation (4), W_m is the function of C and is defined as the concentration of water molecules [31, 33]. In this equation, the non-dimensional parameter represents enthalpy variations of mixing between the water molecules and hydrogel chain with a value of $\chi = 0-1.2$, which expresses the high incentive of water molecules for penetrating the hydrogel network. In the following, T, ν, and K_B are the absolute temperature, the one solvent volume per molecule, and the Boltzmann constant, respectively. It should be noted that the first and last parts of mixing free energy density of the studied multilayer hydrogel $\ln\left(1+\frac{1}{\nu C}\right)$ and $\frac{\chi}{1+\nu C}$ represent the water molecules in polymer chain entropy and mixing enthalpy [90].

Due to the incompressibility at the equilibrium state in any solvent chemical potential, the hydrogel chain volume changes through absorbing, and the excretion of the fluid molecules is constant. The nominal stress tensor (the first Piola-Kirchhoff stress tensor) as the state equation is defined below [27]:

$$\mathbf{P} = \frac{\partial W}{\partial \mathbf{F}} - \frac{\mu}{\nu}\mathbf{I} \qquad (5)$$

In this equation, the considerable point is its negative terminal of $\frac{\mu}{\nu}\mathbf{I}$, which is known as the chemical potential of the hydrogel network (pore pressure in poroelasticity) and applies the hydro-static stress on it. At the equilibrium state, the deformed hydrogel network is affected by the chemical potential. When it is equal to zero, the fluid pressure is the same as vapour pressure. In the mentioned term, $\mathbf{I}$ and μ refer to the identity tensor and the chemical potential of the surrounding water molecules, respectively.

Based on the section about multilayer hydrogel modelling, the swelling mechanism of the submerged hydrogel in the aquatic environment is due to the migration of water molecules into the network. This means any variation in polymer chain stretch referring to the accommodated water molecules into it. It should be noted that the mixing procedure could vary both the entropy and enthalpy of the system in that the contractile stress is the result of declining stretch. In the next stage, the constitutive model for defining multilayer hydrogel swelling behavior is implemented by numerical tools. All the subsequent investigations are simulated by ABAQUS. The nonlinear behavior of smart polymeric materials such as hydrogel in ABAQUS is solved by scripting a UHYPER as a user-defined subroutine in the programming platform to import the boundary conditions. In other words, the swelling behavior of the hydrogel as a hyperelastic material is obtained by calculating the free energy density terms and its derivatives with respect to the deformation gradient invariants in the so-called user-defined subroutine.

As mentioned in the introduction, the present study is inspired by the experimental research by Liu et al. [11]. As can be seen in the micro-channel in Figure 1, the upper side of the channel wall is designed with vertical movement freedom like the channel studied in the mentioned research [11]. In more detailed terms, the moving part of the channel located at the upper side imposes the compression pressure to prevent the passing of any water molecules, thus decreasing the sealing time. It should be noted that each level of pressure from the upper side of the channel wall has a specific indication. For instance, increasing the moving wall compression would mean that higher pressure is required to break the hydrogel. The bottom of the hydrogel rested at the lower surface of the channel. The dimensions of the schematic hydrogel seal (Figure 1) are a thickness (**h**) of **1**, a width of **w**, and a length of **a,** where the channel width in the 2D simulation is adequate. A non-dimensional parameter of Δh/h refers to the strain generated by the upper side of the channel compression (ε) [11]. The model presented above is confirmed by using the elastic model to stimulate the different compression levels.

A neo-Hookean model is used to model the deformation when the seal of the planned test does not swell. The elastomeric seal is compressed via a rigid upper boundary line that moves downward. Similar to the experimental data presented by Liu et al. [11], the contact is assumed to be frictionless. CPE4H and R2D2 mesh types are used to move the boundary line and the elastomer, respectively. A uniformly exerted pressure on the left side of the seal is employed to model the water pressure, which increases linearly until it approaches the maximum contact stress. Although this uniform pressure does not simulate the experiment at first because water exerts pressure on all contactless areas, it is not a serious issue. This is because after a short time, all the upper sides of the seal touch the upper boundary line, and only the left side of the seal is still subjected to the water pressure. Contact stress and water pressure are continuously monitored to report the water pressure that overcomes the contact stress, causing the leakage.

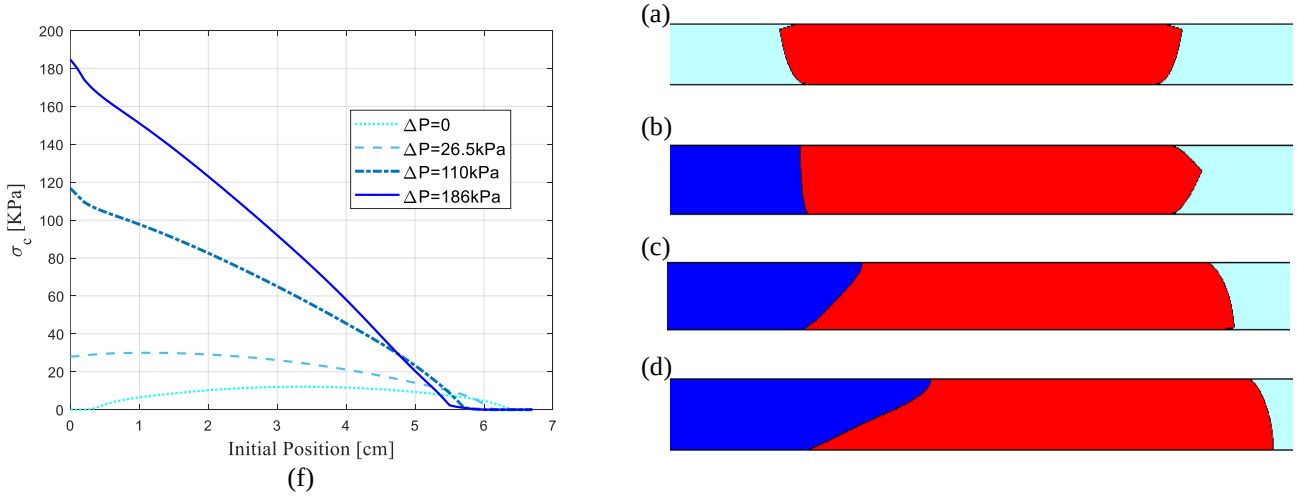

Figure 2: The FEA result of the contact stress versus the initial position in different pressures of 0, 26.5, 110, and 186 kPa. The corresponding deformed configurations are a, b, c, and d, respectively.

FE results were obtained and compared with the experimental and analytical ones. The cross-linking density of this process equals $N\nu = 0.000125$ EEE=10%. The height and three different lengths of the hydrogel are $2.2 \times 4.4 \times 6.7cm$. As mentioned earlier, the friction between the seal and the upper boundary is considered zero.

Figure 2 shows the configurations of the seal with a length of $6.7cm$ subject to different values of pressure. Figure 2(e) shows the contact stress for different values of pressure indicated in Figure 2(a-d). First, the upper boundary line moves down to exert compression on the seal (Figure 2(a)). In Figure 2 (b-d), the left side of the seal is influenced by

the pressure, resulting in deformation and contact stress growth. The maximum contact stress is observed at the midpoint of the seal. Exerting pressure on the left side of the seal increases the maximum contact stress, and it starts to move to the end of the seal. When it coincides with the endpoint of the seal, the maximum contact stress only increases in magnitude. The mentioned process is slower than increasing the fluid pressure and continues until the exerted pressure overcomes the contact stress that initiates the leakage.

3. Leak by Pressure

When a seal is placed in its working environment, it exerts pressure on the channel walls that is larger than the surrounding fluid pressure. Therefore, the fluid cannot separate the seal from the wall and thus cannot leak. If the pressure of fluid increases and becomes higher than the contact pressure, the flow overcomes the barrier and leaks by creating a leakage path through the seal, removing it from its place, or rupturing it. The investigations in this study consider the elastic failure of seals, which is the most common type of failure for such seals [20]. In elastic failure, the seal is not damaged or removed from its position, but the large elastic deformation reduces the contact pressure (stress) and leads to leakage. This is a reversible process, and the seal can perform once the pressure of the fluid is decreased.

There are various methods of creating the initial contact pressure necessary for sealing. In swellable seals, the hydrogels absorb water, swell, generate contact with the channel walls, and produce the necessary contact pressure. Initially, in rectangular seals, the contact pressure is symmetrical and higher at the middle of the hydrogel and gradually decreases as it distances from the middle of the hydrogel. When subjected to fluid pressure, the seal is deformed, and the symmetry in the distribution of the contact pressure is impaired. The position of maximum contact pressure moves to the side with fluid pressure [13]. If the pressure continues to rise in the fluid, the contact pressure moves further toward that side. It should be noted that, as shown later, the value of contact pressure is not constant and changes with the deformation of the hydrogel. At some point, the fluid pressure exceeds the contact pressure, and the hydrogel fails to seal the channel, initiating the leakage path [35].

4. A detailed study of the rectangular multilayer hydrogel seal

This paper used the Finite Element Method (FEM) to investigate the behavior of the proposed seal. A UHYPER subroutine was introduced to import the material properties to ABAQUS software in which the energy parameter and its derivatives with respect to the deformation gradient invariants were scripted. In the ABAQUS software, the CPE4H mesh model is selected for the problem simulation, where the length of the multilayer seal is considered sufficient as a 2D problem. The FE model performs like the mentioned model with which it was validated. However, it should be noted that the material model and the movement of the upper boundary condition are different in the current work compared to the validation one.

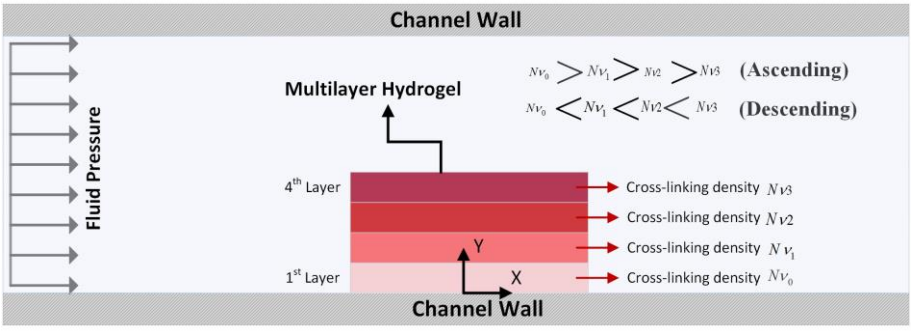

Figure 3: The multilayer hydrogel seals schematic alongside two methods for the cross-linking density.

The length and thickness of the multilayer seal are 40 and 20 mm, respectively, except for the parametric studies where the mentioned values are changed. This multilayer has been implemented in a channel with a width of 30 mm. It is assumed that the interaction parameter is 0.6, and the cross-linking density ranges from 0.005 to 0.02 for the multilayer cases (Figure 3). Figure 4 shows the formation of the system for the descending cross-linking distribution in different steps. First, the configuration of the undeformed multilayer seal is shown in Figure 4(a). Figure 4 (b) shows the seal position when the swelling procedure is completed, but the external pressure is not exerted yet. In

Figure 4(c) and 4(f), different pressures of 380, 800, 1580, and 2600kPa are exerted on the left side of the seal. The leakage occurs when the pressure equals 2600 kPa (Figure 4 (f)). Von Mises stress contour is also shown in Figure 4. In Figure 4(b), when the seal is in the swelled configuration, the external pressure is observed at the corner points of the lowest side of the seal where it is attached to the wall. As shown in Figures 4(c) and 4(d), the maximum value is first on the high-pressure and then begins to increase owing to the multilayer deformation.

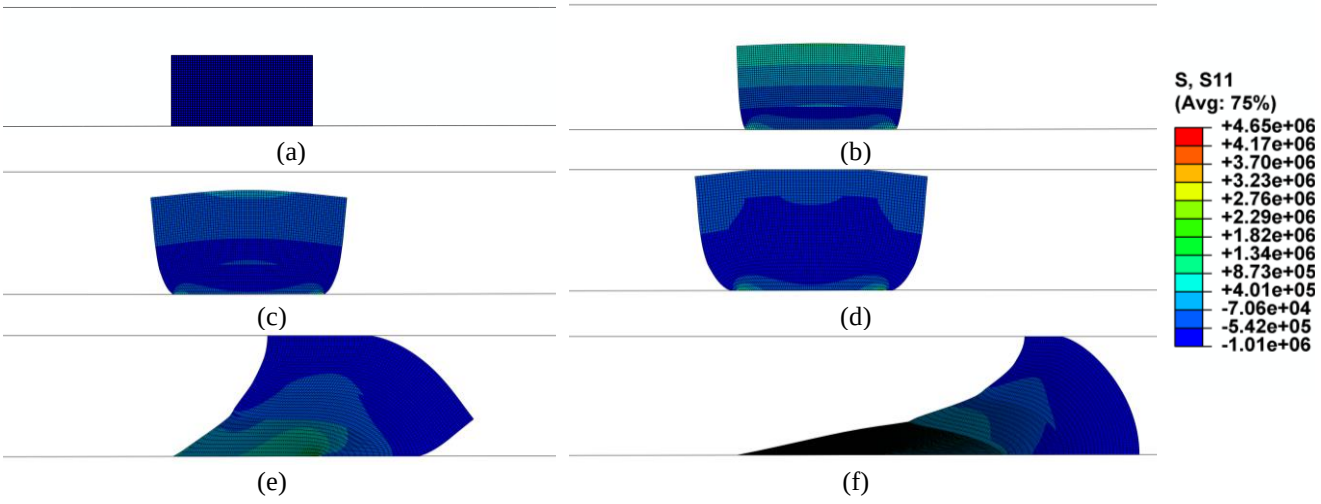

Figure 4: FEM results of understudy multilayer hydrogel in different pressures.

Increasing the fluid pressure causes the elements located on the left side to approach their initial positions so that their stretches reduce. However, when pressure exceeds a particular value, those elements start to distance, leading their stretch to extend again. It should be noted that on the right side of the seal, von Mises stress is continuously rising. Also, mesh independency is an important factor in FE simulations due to reaching precise results by optimized computational costs. Afterward, the mesh size does not affect the multilayer hydrogel results. As illustrated in Figure 5: Independency of the understudy hydrogel seal for the number of elements versus obtained tolerable pressure for descending material distribution., for the subsequent analysis of the multilayer in both ascending and descending states, the number of elements is considered 2290, where the obtained result had no fluctuation.

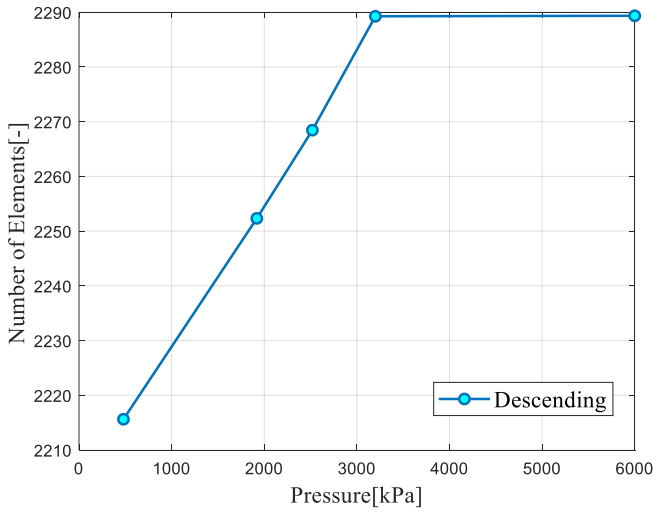

Figure 5: Independency of the understudy hydrogel seal for the number of elements versus obtained tolerable pressure for descending material distribution.

For clarification, Figure 4 presents the contact stress between the seal and the channel wall. As can be seen, initially, a completely symmetrical contact stress profile is observed where the maximum level of contact stress is at the center of the multilayer and is zero at the two contact ends. It should be noted that at first, the contact end does not occur simultaneously with the seal corners, which means that the outer parts of the seal do not touch the upper wall. While the fluid flow pressure increases, the seal begins to deform slowly, and before the fluid pressure reaches the maximum contact stress, the maximum points approach the corner of the seal. When this corner touches the upper wall and matches the location of the maximum contact stress, the pressure grows with a much sharper slope than in other areas. Thus, even if the fluid pressure is higher than the contact stress for most contact areas, the seal prevents leakage, as the fluid pressure is lower than the contact stress in this particular area. However, when the external pressure exceeds the contact stress of this area, the system fails and leads to leakage. This sudden leakage was also observed in articles [11, 67]. This deformation can also affect the right side of the seal as the contact surface is reduced. As the pressure difference increases, the contact surface of the right side is decreased.

5. Parametric investigation

In this section, the parameters that have a significant effect on the behavior of the multilayer are studied. The effect of the multilayer length and the ratio of the multilayer thickness to the gap (RTG) of seals are studied. The effect of the cross-linking density (Nv) is also investigated, where the amount of this parameter is constant through the seal (homogenous cases). For multilayer seals, both ascending and descending arrangements are considered where the cross-linking density increases and decreases from the top to the bottom, respectively. The reason for investigating the multilayer length is that it can affect contact stress and the amount of deformation. The RTG parameter is significant not only in the initial contact stress but also in design limitations. As concluded from the model description, the cross-linking density affects the multilayer behavior significantly, particularly the amount of swelling and contact stress.

5.1. Multilayer length

In this section, the impact of the multilayer length is studied for ascending and descending cases. The multilayer thickness, channel width, and interaction parameters have constant values of 20mm, 30 mm, and 0.6, respectively. As can be seen in Figure 6, for both ascending and descending arrangements, increasing the multilayer length increases its capability to endure the pressure difference in nearly-linear trends. This outcome can be described through the deformation mechanism of the multilayer, as a multilayer with a longer length has a higher impediment to deformation. When the multilayer length increases, pressure on the wall and the contact stress increase, resulting in a higher-pressure difference. It should be noted that the ascending case is more affected by the length than the descending.

5.2. The ratio of the multilayer thickness to the gap (RTG)

The RTG parameter has a great impact on the seal performance and is governed by design limitations and the place of the multilayer. In this study, the RTG parameter depends on multilayer thickness only as the channel width is fixed. In the present study, the multilayer length, channel width, and interaction parameters have constant values of 40mm, 30mm, and 0.6, respectively. Figure 7 shows the effect of this parameter on the behavior of ascending and descending multilayers. As can be seen, similar to the length study, by increasing the RTG parameter, the resistance of the multilayer increases in a linear way for ascending and descending arrangements. Another conclusion from the two mentioned parametric studies is that, on the whole, the multilayers with descending arrangements have a better ability to resist pressure difference than layers with ascending arrangements.

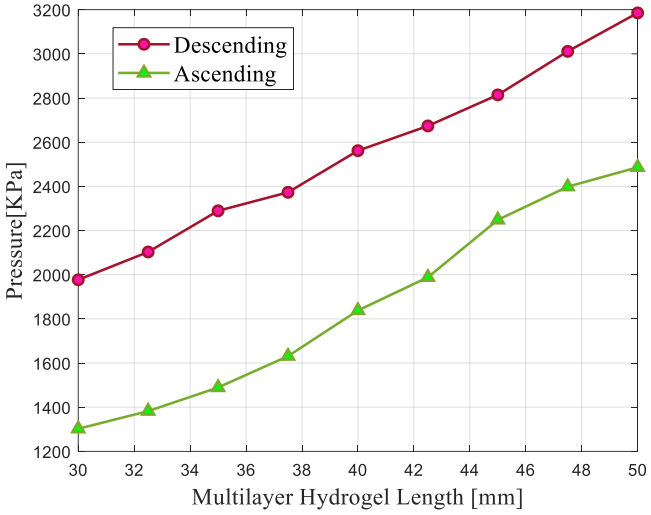

Figure 6: The Obtained maximum results of tolerable pressure according to multilayer hydrogel length variation.

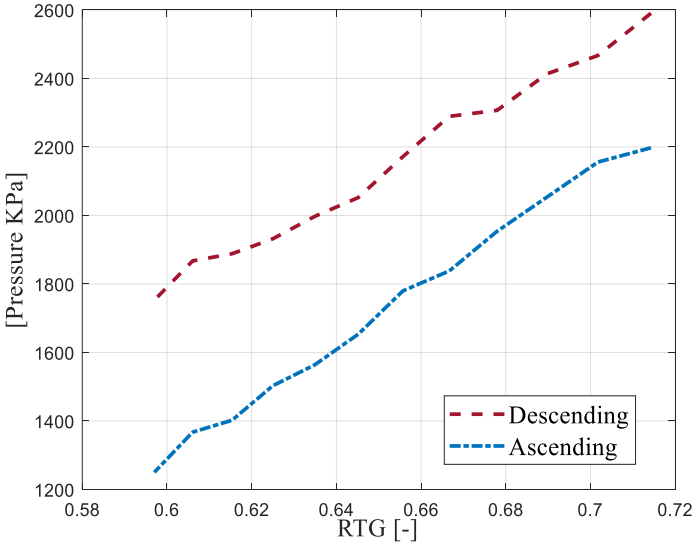

Figure 7: RTG effect of the ascending and descending method of multilayer cross-linking on the tolerable pressure.

5.3. Cross-linking density for homogenous hydrogel

Another important parameter in the sealing system is the cross-linking density ($N\nu$). Four homogenous seals with different Nv values (0.005, 0.01, 0.015, and 0.02) are considered to investigate this parameter, and the results are presented in Table 1. As expected, the seal with a higher Nv can resist a higher pressure difference. This observation is the outcome of higher stiffness in seals with more amounts of Nv, resulting in better resistance to deformation.

Table 1: Pressure leakage of homogeneous hydrogels

Cross-linking density	Pressure (KPa)
$N\nu = 0.005$	1120.954
$N\nu = 0.01$	2002.969
$N\nu = 0.015$	2757.073
$N\nu = 0.02$	3372.951

6. Summary and Conclusion

The present study investigated the performance of multilayer hydrogel seals. The behavior of hydrogel encounters with the pressure profile of fluid flow was assessed using a suitable constitutive model and elastic leakage method to analyze the sealing behavior of the hydrogel. The mentioned model helped consider different aspects of hydrogel behavior, including the generated stress in the rectangular multilayer hydrogel, the contact stress, and the deformed configuration. The hydrogel in rectangular shape was reconstructed in four layers, where the amount of cross-linking decreased from the top to the bottom of the hydrogel as the descending distribution and increased from the top to the bottom of the hydrogel as ascending distribution. Afterward, more than 50 simulations were performed as parameter studies to demonstrate the precise approach to designing such elastomeric seals. The investigated parameter study contains the variation of hydrogel length for ascending and descending cross-linking density distributions and material property distribution (amount of *Nv*) and measures the amount of pressure before the failure of the RTG (the ratio of the thickness of the hydrogel to the gap). It is defined as a geometrical parameter that has been studied comprehensively. For the RTG, the results demonstrated that as the hydrogel seal length increases, the capacity of the pressure before the hydrogel failure (i.e., the ratio of the thickness of the hydrogel to the gap) is increased. The pressure-bearing of the multilayer hydrogel with descending cross-linking distribution is 1.5 times higher than the ascending state.

References

[1] J. Wu, Z.-G. Su, G.-H. Ma, A thermo-and pH-sensitive hydrogel composed of quaternized chitosan/glycerophosphate, *International journal of pharmaceutics*, Vol. 315, No. 1-2, pp. 1-11, 2006.

[2] A. Suzuki, S. Yoshikawa, G. Bai, Shrinking pattern and phase transition velocity of poly (N-isopropylacrylamide) gel, *The Journal of chemical physics*, Vol. 111, No. 1, pp. 360-367, 1999.

[3] D. J. Beebe, J. S. Moore, J. M. Bauer, Q. Yu, R. H. Liu, C. Devadoss, B.-H. Jo, Functional hydrogel structures for autonomous flow control inside microfluidic channels, *Nature*, Vol. 404, No. 6778, pp. 588-590, 2000.

[4] D. T. Eddington, D. J. Beebe, Flow control with hydrogels, *Advanced drug delivery reviews*, Vol. 56 2, pp. 199-210, 2004.

[5] Y. Zhang, Z. Liu, S. Swaddiwudhipong, H. Miao, Z. Ding, Z. Yang, pH-sensitive hydrogel for micro-fluidic valve, *Journal of Functional Biomaterials*, Vol. 3, No. 3, pp. 464-479, 2012.

[6] W. Toh, T. Y. Ng, J. Hu, Z. Liu, Mechanics of inhomogeneous large deformation of photo-thermal sensitive hydrogels, *International Journal of Solids and Structures*, Vol. 51, No. 25-26, pp. 4440-4451, 2014.

[7] H. Mazaheri, A. H. Namdar, A. Ghasemkhani, A model for inhomogeneous large deformation of photo-thermal sensitive hydrogels, *Acta Mechanica*, pp. 1-18, 2021.

[8] H. Mazaheri, A. Ghasemkhani, A. Namdar, Behavior of photo-thermal sensitive polyelectrolyte hydrogel micro-valve: analytical and numerical approaches, *Journal of Stress Analysis*, Vol. 5, No. 1, pp. 21-30, 2020.

[9] W. Shi, J. Huang, R. Fang, M. Liu, Imparting functionality to the hydrogel by magnetic-field-induced nano-assembly and macro-response, *ACS applied materials & interfaces*, Vol. 12, No. 5, pp. 5177-5194, 2020.

[10] M. N. Hsu, S. C. Wei, S. Guo, D. T. Phan, Y. Zhang, C. H. Chen, Smart hydrogel microfluidics for single-cell multiplexed secretomic analysis with high sensitivity, *Small*, Vol. 14, No. 49, pp. 1802918, 2018.

[11] Q. Liu, Z. Wang, Y. Lou, Z. Suo, Elastic leak of a seal, *Extreme Mechanics Letters*, Vol. 1, pp. 54-61, 2014.

[12] R. Geryak, V. V. Tsukruk, Reconfigurable and actuating structures from soft materials, *Soft Matter*, Vol. 10, No. 9, pp. 1246-1263, 2014.

[13] H. Banerjee, M. Suhail, H. Ren, Hydrogel Actuators and Sensors for Biomedical Soft Robots: Brief Overview with Impending Challenges, *Biomimetics*, Vol. 3, No. 3, pp. 15, 2018.

[14] B. Chen, C. Chen, Y. Lou, Z. Suo, Strain-stiffening seal, *Soft Matter*, Vol. 18, No. 15, pp. 2992-3003, 2022.

[15] H. Mazaheri, A. Khodabandehloo, FSI and non-FSI studies on a functionally graded temperature-responsive hydrogel bilayer in a micro-channel, *Smart Materials and Structures*, 2021.

[16] A. Ghasemkhani, H. Mazaheri, A. Amiri, Fluid-structure interaction simulations for a temperature-sensitive functionally graded hydrogel-based micro-channel, *Journal of Intelligent Material Systems and Structures*, Vol. 32, No. 6, pp. 661-677, 2021.

[17] H. Mazaheri, A. Ghasemkhani, S. Sabbaghi, Study of Fluid–Structure Interaction in a Functionally Graded pH-Sensitive Hydrogel Micro-Valve, *International Journal of Applied Mechanics*, Vol. 12, No. 05, pp. 2050057, 2020.

[18] H. Mazaheri, A. Namdar, A. Amiri, Behavior of a smart one-way micro-valve considering fluid–structure interaction, *Journal of Intelligent Material Systems and Structures*, Vol. 29, No. 20, pp. 3960-3971, 2018.

[19] H. Mazaheri, A. Khodabandehloo, Behavior of an FG temperature-responsive hydrogel bilayer: Analytical and numerical approaches, *Composite Structures*, Vol. 301, pp. 116203, 2022/12/01/, 2022.

[20] M. Mohammadi, A. Farajpour, A. Moradi, M. Hosseini, Vibration analysis of the rotating multilayer piezoelectric Timoshenko nanobeam, *Engineering Analysis with Boundary Elements*, Vol. 145, pp. 117-131, 2022.

[21] M. Mohammadi, A. Rastgoo, Primary and secondary resonance analysis of FG/lipid nanoplate with considering porosity distribution based on a nonlinear elastic medium, *Mechanics of Advanced Materials and Structures*, Vol. 27, No. 20, pp. 1709-1730, 2020.

[22] M. Mohammadi, A. Farajpour, A. Rastgoo, Coriolis effects on the thermo-mechanical vibration analysis of the rotating multilayer piezoelectric nanobeam, *Acta Mechanica*, https://doi.org/10.1007/s00707-022-03430-0, 2023.

[23] M. Mohammadi, M. Hosseini, M. Shishesaz, A. Hadi, A. Rastgoo, Primary and secondary resonance analysis of porous functionally graded nanobeam resting on a nonlinear foundation subjected to mechanical and electrical loads, *European Journal of Mechanics-A/Solids*, Vol. 77, pp. 103793, 2019.

[24] M. Mohammadi, A. Rastgoo, Nonlinear vibration analysis of the viscoelastic composite nanoplate with three directionally imperfect porous FG core, *Structural Engineering and Mechanics, An Int'l Journal*, Vol. 69, No. 2, pp. 131-143, 2019.

[25] A. Farajpour, A. Rastgoo, M. Mohammadi, Vibration, buckling and smart control of microtubules using piezoelectric nanoshells under electric voltage in thermal environment, *Physica B: Condensed Matter*, Vol. 509, pp. 100-114, 2017.

[26] A. Farajpour, M. H. Yazdi, A. Rastgoo, M. Loghmani, M. Mohammadi, Nonlocal nonlinear plate model for large amplitude vibration of magneto-electro-elastic nanoplates, *Composite Structures*, Vol. 140, pp. 323-336, 2016.

[27] A. Farajpour, M. Yazdi, A. Rastgoo, M. Mohammadi, A higher-order nonlocal strain gradient plate model for buckling of orthotropic nanoplates in thermal environment, *Acta Mechanica*, Vol. 227, No. 7, pp. 1849-1867, 2016.

[28] M. Mohammadi, M. Safarabadi, A. Rastgoo, A. Farajpour, Hygro-mechanical vibration analysis of a rotating viscoelastic nanobeam embedded in a visco-Pasternak elastic medium and in a nonlinear thermal environment, *Acta Mechanica*, Vol. 227, No. 8, pp. 2207-2232, 2016.

[29] M. R. Farajpour, A. Rastgoo, A. Farajpour, M. Mohammadi, Vibration of piezoelectric nanofilm-based electromechanical sensors via higher-order non-local strain gradient theory, *Micro & Nano Letters*, Vol. 11, No. 6, pp. 302-307, 2016.

[30] M. Baghani, M. Mohammadi, A. Farajpour, Dynamic and stability analysis of the rotating nanobeam in a nonuniform magnetic field considering the surface energy, *International Journal of Applied Mechanics*, Vol. 8, No. 04, pp. 1650048, 2016.

[31] M. Goodarzi, M. Mohammadi, M. Khooran, F. Saadi, Thermo-mechanical vibration analysis of FG circular and annular nanoplate based on the visco-pasternak foundation, *Journal of Solid Mechanics*, Vol. 8, No. 4, pp. 788-805, 2016.

[32] H. Asemi, S. Asemi, A. Farajpour, M. Mohammadi, Nanoscale mass detection based on vibrating piezoelectric ultrathin films under thermo-electro-mechanical loads, *Physica E: Low-dimensional Systems and Nanostructures*, Vol. 68, pp. 112-122, 2015.

[33] M. Safarabadi, M. Mohammadi, A. Farajpour, M. Goodarzi, Effect of surface energy on the vibration analysis of rotating nanobeam, 2015.

[34] M. Goodarzi, M. Mohammadi, A. Gharib, Techno-Economic Analysis of Solar Energy for Cathodic Protection of Oil and Gas Buried Pipelines in Southwestern of Iran, in *Proceeding of*, https://publications.waset.org/abstracts/33008/techno-economic-analysis-of …, pp.

[35] M. Mohammadi, A. A. Nekounam, M. Amiri, The vibration analysis of the composite natural gas pipelines in the nonlinear thermal and humidity environment, in *Proceeding of*, https://civilica.com/doc/540946/, pp.

[36] M. Goodarzi, M. Mohammadi, M. Rezaee, Technical Feasibility Analysis of PV Water Pumping System in Khuzestan Province-Iran, in *Proceeding of*, https://publications.waset.org/abstracts/18930/technical-feasibility …, pp.

[37] M. Mohammadi, A. Farajpour, A. Moradi, M. Ghayour, Shear buckling of orthotropic rectangular graphene sheet embedded in an elastic medium in thermal environment, *Composites Part B: Engineering*, Vol. 56, pp. 629-637, 2014.

[38] M. Mohammadi, A. Moradi, M. Ghayour, A. Farajpour, Exact solution for thermo-mechanical vibration of orthotropic mono-layer graphene sheet embedded in an elastic medium, *Latin American Journal of Solids and Structures*, Vol. 11, pp. 437-458, 2014.

[39] M. Mohammadi, A. Farajpour, M. Goodarzi, F. Dinari, Thermo-mechanical vibration analysis of annular and circular graphene sheet embedded in an elastic medium, *Latin American Journal of Solids and Structures*, Vol. 11, pp. 659-682, 2014.

[40] M. Mohammadi, A. Farajpour, M. Goodarzi, Numerical study of the effect of shear in-plane load on the vibration analysis of graphene sheet embedded in an elastic medium, *Computational Materials Science*, Vol. 82, pp. 510-520, 2014.

[41] A. Farajpour, A. Rastgoo, M. Mohammadi, Surface effects on the mechanical characteristics of microtubule networks in living cells, *Mechanics Research Communications*, Vol. 57, pp. 18-26, 2014.

[42] S. R. Asemi, M. Mohammadi, A. Farajpour, A study on the nonlinear stability of orthotropic single-layered graphene sheet based on nonlocal elasticity theory, *Latin American Journal of Solids and Structures*, Vol. 11, pp. 1541-1546, 2014.

[43] M. Goodarzi, M. Mohammadi, A. Farajpour, M. Khooran, Investigation of the effect of pre-stressed on vibration frequency of rectangular nanoplate based on a visco-Pasternak foundation, 2014.

[44] S. Asemi, A. Farajpour, H. Asemi, M. Mohammadi, Influence of initial stress on the vibration of double-piezoelectric-nanoplate systems with various boundary conditions using DQM, *Physica E: Low-dimensional Systems and Nanostructures*, Vol. 63, pp. 169-179, 2014.

[45] S. Asemi, A. Farajpour, M. Mohammadi, Nonlinear vibration analysis of piezoelectric nanoelectromechanical resonators based on nonlocal elasticity theory, *Composite Structures*, Vol. 116, pp. 703-712, 2014.

[46] M. Mohammadi, M. Ghayour, A. Farajpour, Free transverse vibration analysis of circular and annular graphene sheets with various boundary conditions using the nonlocal continuum plate model, *Composites Part B: Engineering*, Vol. 45, No. 1, pp. 32-42, 2013.

[47] M. Mohammadi, M. Goodarzi, M. Ghayour, A. Farajpour, Influence of in-plane pre-load on the vibration frequency of circular graphene sheet via nonlocal continuum theory, *Composites Part B: Engineering*, Vol. 51, pp. 121-129, 2013.

[48] M. Mohammadi, A. Farajpour, M. Goodarzi, R. Heydarshenas, Levy type solution for nonlocal thermo-mechanical vibration of orthotropic mono-layer graphene sheet embedded in an elastic medium, *Journal of Solid Mechanics*, Vol. 5, No. 2, pp. 116-132, 2013.

[49] M. Mohammadi, A. Farajpour, M. Goodarzi, H. Mohammadi, Temperature Effect on Vibration Analysis of Annular Graphene Sheet Embedded on Visco-Pasternak Foundati, *Journal of Solid Mechanics*, Vol. 5, No. 3, pp. 305-323, 2013.

[50] M. Danesh, A. Farajpour, M. Mohammadi, Axial vibration analysis of a tapered nanorod based on nonlocal elasticity theory and differential quadrature method, *Mechanics Research Communications*, Vol. 39, No. 1, pp. 23-27, 2012.

[51] A. Farajpour, A. Shahidi, M. Mohammadi, M. Mahzoon, Buckling of orthotropic micro/nanoscale plates under linearly varying in-plane load via nonlocal continuum mechanics, *Composite Structures*, Vol. 94, No. 5, pp. 1605-1615, 2012.

[52] M. Mohammadi, M. Goodarzi, M. Ghayour, S. Alivand, Small scale effect on the vibration of orthotropic plates embedded in an elastic medium and under biaxial in-plane pre-load via nonlocal elasticity theory, 2012.

[53] A. Farajpour, M. Mohammadi, A. Shahidi, M. Mahzoon, Axisymmetric buckling of the circular graphene sheets with the nonlocal continuum plate model, *Physica E: Low-dimensional Systems and Nanostructures*, Vol. 43, No. 10, pp. 1820-1825, 2011.

[54] A. Farajpour, M. Danesh, M. Mohammadi, Buckling analysis of variable thickness nanoplates using nonlocal continuum mechanics, *Physica E: Low-dimensional Systems and Nanostructures*, Vol. 44, No. 3, pp. 719-727, 2011.

[55] H. Moosavi, M. Mohammadi, A. Farajpour, S. Shahidi, Vibration analysis of nanorings using nonlocal continuum mechanics and shear deformable ring theory, *Physica E: Low-dimensional Systems and Nanostructures,* Vol. 44, No. 1, pp. 135-140, 2011.

[56] M. Mohammadi, M. Ghayour, A. Farajpour, Analysis of free vibration sector plate based on elastic medium by using new version differential quadrature method, *Journal of solid mechanics in engineering,* Vol. 3, No. 2, pp. 47-56, 2011.

[57] A. Farajpour, M. Mohammadi, M. Ghayour, Shear buckling of rectangular nanoplates embedded in elastic medium based on nonlocal elasticity theory, in *Proceeding of,* www.civilica.com/Paper-ISME19-ISME19_390.html, pp. 390.

[58] M. Mohammadi, A. Farajpour, A. R. Shahidi, Higher order shear deformation theory for the buckling of orthotropic rectangular nanoplates using nonlocal elasticity, in *Proceeding of,* www.civilica.com/Paper-ISME19-ISME19_391.html, pp. 391.

[59] M. Mohammadi, A. Farajpour, A. R. Shahidi, Effects of boundary conditions on the buckling of single-layered graphene sheets based on nonlocal elasticity, in *Proceeding of,* www.civilica.com/Paper-ISME19-ISME19_382.html, pp. 382.

[60] M. Mohammadi, M. Ghayour, A. Farajpour, Using of new version integral differential method to analysis of free vibration orthotropic sector plate based on elastic medium, in *Proceeding of,* www.civilica.com/Paper-ISME19-ISME19_497.html, pp. 497.

[61] N. Ghayour, A. Sedaghat, M. Mohammadi, Wave propagation approach to fluid filled submerged visco-elastic finite cylindrical shells, 2011.

[62] N. A. Peppas, J. Z. Hilt, A. Khademhosseini, R. Langer, Hydrogels in Biology and Medicine: From Molecular Principles to Bionanotechnology, *Advanced Materials,* Vol. 18, No. 11, pp. 1345-1360, 2006.

[63] R. Noroozi, M. A. Shamekhi, R. Mahmoudi, A. Zolfagharian, F. Asgari, A. Mousavizadeh, M. Bodaghi, A. Hadi, N. Haghighipour, In vitro static and dynamic cell culture study of novel bone scaffolds based on 3D-printed PLA and cell-laden alginate hydrogel, *Biomedical Materials,* Vol. 17, No. 4, pp. 045024, 2022/06/22, 2022.

[64] G. Chan, D. J. Mooney, New materials for tissue engineering: towards greater control over the biological response, *Trends in biotechnology,* Vol. 26, No. 7, pp. 382-392, 2008.

[65] R. Noroozi, F. Tatar, A. Zolfagharian, R. Brighenti, M. A. Shamekhi, A. Rastgoo, A. Hadi, M. Bodaghi, Additively manufactured multi-morphology bone-like porous scaffolds: experiments and micro-computed tomography-based finite element modeling approaches, *International Journal of Bioprinting,* Vol. 8, No. 3, pp. 40-53, 2022.

[66] Z. U. Arif, M. Y. Khalid, R. Noroozi, A. Sadeghianmaryan, M. Jalalvand, M. Hossain, Recent advances in 3D-printed polylactide and polycaprolactone-based biomaterials for tissue engineering applications, *International Journal of Biological Macromolecules*, 2022.

[67] B. Druecke, E. Dussan V, N. Wicks, A. Hosoi, Large elastic deformation as a mechanism for soft seal leakage, *Journal of Applied Physics,* Vol. 117, No. 10, pp. 104511, 2015.

[68] S. K. S. Kambhammettu, L. R. Chebolu, A. P. Deshpande, A wedge penetration model to estimate leak through elastomer–metal interface, *International Journal of Advances in Engineering Sciences and Applied Mathematics,* Vol. 12, No. 1, pp. 65-72, 2020.

[69] T. T. Hailey Jr, R. Freyer, Well tools with actuators utilizing swellable materials, Google Patents, 2013.

[70] J. Kluge, B. Jansen, A. Lutz, D. K. De, W. S. Butterfield, P. Williamson, Downwell system with activatable swellable packer, Google Patents, 2009.

[71] S. Cai, Z. Suo, Mechanics and chemical thermodynamics of phase transition in temperature-sensitive hydrogels, *Journal of the Mechanics and Physics of Solids,* Vol. 59, No. 11, pp. 2259-2278, 2011.

[72] S. A. Chester, L. Anand, A coupled theory of fluid permeation and large deformations for elastomeric materials, *Journal of the Mechanics and Physics of Solids,* Vol. 58, No. 11, pp. 1879-1906, 2010.

[73] H. Mazaheri, M. Baghani, R. Naghdabadi, S. Sohrabpour, Inhomogeneous swelling behavior of temperature sensitive PNIPAM hydrogels in micro-valves: analytical and numerical study, *Smart Materials and Structures,* Vol. 24, No. 4, pp. 045004, 2015.

[74] A. Drozdov, J. deClaville Christiansen, Time-dependent response of hydrogels under multiaxial deformation accompanied by swelling, *Acta Mechanica,* Vol. 229, No. 12, pp. 5067-5092, 2018.

[75] W. Hong, X. Zhao, J. Zhou, Z. Suo, A theory of coupled diffusion and large deformation in polymeric gels, *Journal of the Mechanics and Physics of Solids,* Vol. 56, No. 5, pp. 1779-1793, 2008.

[76] P. J. Flory, J. Rehner Jr, Statistical mechanics of cross-linked polymer networks I. Rubberlike elasticity, *The journal of chemical physics,* Vol. 11, No. 11, pp. 512-520, 1943.

[77] P. J. Flory, Thermodynamics of high polymer solutions, *The Journal of chemical physics,* Vol. 10, No. 1, pp. 51-61, 1942.

[78] M. L. Huggins, Some properties of solutions of long-chain compounds, *The Journal of Physical Chemistry,* Vol. 46, No. 1, pp. 151-158, 1942.

[79] Y. Lou, S. Chester, Kinetics of swellable packers under downhole conditions, *International Journal of Applied Mechanics,* Vol. 6, No. 06, pp. 1450073, 2014.

[80] Q. Liu, A. Robisson, Y. Lou, Z. Suo, Kinetics of swelling under constraint, *Journal of Applied Physics,* Vol. 114, No. 6, pp. 064901, 2013.

[81] Z. Wang, C. Chen, Q. Liu, Y. Lou, Z. Suo, Extrusion, slide, and rupture of an elastomeric seal, *Journal of the Mechanics and Physics of Solids,* Vol. 99, pp. 289-303, 2017.

[82] Y. Lou, A. Robisson, S. Cai, Z. Suo, Swellable elastomers under constraint, *Journal of Applied Physics,* Vol. 112, No. 3, pp. 034906, 2012.

[83] N. Arbabi, M. Baghani, J. Abdolahi, H. Mazaheri, M. M. Mashhadi, Finite bending of bilayer pH-responsive hydrogels: a novel analytic method and finite element analysis, *Composites Part B: Engineering,* Vol. 110, pp. 116-123, 2017.

[84] J. Abdolahi, M. Baghani, N. Arbabi, H. Mazaheri, Finite bending of a temperature-sensitive hydrogel tri-layer: An analytical and finite element analysis, *Composite Structures,* Vol. 164, pp. 219-228, 2017/03/15/, 2017.

[85] H. Mazaheri, A. Ghasemkhani, Analytical and numerical study of the swelling behavior in functionally graded temperature-sensitive hydrogel shell, *Journal of Stress Analysis,* Vol. 3, No. 2, pp. 29-35, 2019.

[86] a. h. namdar, Kinetics of swelling of cylindrical functionally graded temperature-responsive hydrogels, *Journal of Computational Applied Mechanics,* Vol. 51, No. 2, pp. 464-471, 2020.

[87] A. Khodabandehloo, H. Mazaheri, Analytic and Finite Element Studies on Deformation of Bilayers with a Functionally Graded PH-Responsive Hydrogel Layer, *International Journal of Applied Mechanics,* Vol. 0, No. 0, pp. 2250053.

[88] H. Mazaheri, K. Soleymani, A. Ghasemkhani, An Analytical Solution and FEM Simulation for the Behavior of Sensitive FG micro-valve in Response to pH Stimuli, *Journal of Stress Analysis,* Vol. 6, No. 1, pp. -, 2021.

[89] A. H. Namdar, H. Mazaheri, Kinetics of swelling of cylindrical temperature-responsive hydrogel: a semi-analytical study, *International Journal of Applied Mechanics,* Vol. 12, No. 08, pp. 2050090, 2020.

[90] W. Hong, Z. Liu, Z. Suo, Inhomogeneous swelling of a gel in equilibrium with a solvent and mechanical load, *International Journal of Solids and Structures,* Vol. 46, No. 17, pp. 3282-3289, 2009.